

Zirconia-germanium interface photoemission spectroscopy using synchrotron radiation

Chi On Chui^{a)}

Department of Electrical Engineering, Stanford University, Stanford, California 94305

Dong-Ick Lee, Andy A. Singh, and Piero A. Pianetta

Stanford Synchrotron Radiation Laboratory, Stanford University, Stanford, California 94309

Krishna C. Saraswat

Department of Electrical Engineering, Stanford University, Stanford, California 94305

(Received 23 December 2004; accepted 29 March 2005; published online 27 May 2005)

An *ultrathin* zirconia gate dielectric had been successfully incorporated into germanium metal-oxide-semiconductor (MOS) devices demonstrating very high-permittivity gate stacks with no apparent interfacial layer. In this study, synchrotron-radiation photoemission spectroscopy has been applied on the same gate stack to identify and quantify the presence of any interfacial germanium suboxide layer. By taking progressive core-level spectra during the layer-by-layer removal of the zirconia film, an oxidized germanium layer with submonolayer thickness was found, possibly arising from an interfacial Zr–O–Ge bonding configuration. In addition, the offsets in the valence-band spectra were also monitored and the energy-band diagram of the zirconia–germanium heterostructure was constructed. Compared to high- κ gate stacks on Si, the thinner interfacial layer and larger conduction-band offset in high- κ gate stacks on Ge suggest better scalability towards an ultimately higher MOS gate capacitance. © 2005 American Institute of Physics.

[DOI: 10.1063/1.1922090]

I. INTRODUCTION

As the scaling of the classical bulk silicon (Si) metal-oxide-semiconductor field-effect transistors (MOSFETs) approaches its fundamental limits, innovative device structures and new materials¹ are needed to continue the historic progress in information processing and transmission. Among various high mobility channel candidates, germanium (Ge) has recently been suggested^{1–4} to alleviate the problem of MOSFET drain current saturation by providing a higher source injection velocity.⁵ Historically, Ge had been one of the most important semiconductors, and the instability of native Ge oxides (GeO_x) was one of the key enablers in the first (point-contact) transistor demonstration.⁶ On the other hand, its inferior properties, especially when compared to silicon dioxide, makes this dielectric unsuitable for Ge MOSFET gate insulation and field isolation, and has therefore prevented very large-scale integration (VLSI) of Ge devices for decades.

Before the interest in Ge as a channel material for decanano-scale MOSFETs could be facilitated, a stable as well as scalable gate dielectric technology has to be developed. The feasibility of employing high-permittivity (high- κ) metal oxide dielectrics to satisfy both criteria simultaneously have previously been suggested.^{3,7} Usually, such high- κ dielectric integration to Si inherits a lower-permittivity Si suboxide (SiO_x) interfacial layer between the high- κ film and the Si substrate,⁸ which is currently the major bottleneck to scale the gate-stack-equivalent silicon dioxide thickness

(EOT) thinner than 1.3 nm.¹ For Ge, conversely, the thermodynamic instability of GeO_x may permit a true high- κ gate stack on Ge without a lower-permittivity interfacial layer, and thereby break through the EOT scaling barrier. For instance, a sub-1.0-nm EOT zirconia (ZrO₂) on Ge gate stack⁷ revealed no apparent interfacial layer in between as illustrated in Fig. 1. Nonetheless, the conventional transmission electron microscopy (TEM) is not well suited for identifying an interfacial GeO_x layer in this material system due to the closeness in atomic number of zirconium (Zr) and Ge, resulting in poor image contrast.

In order to understand whether it is technologically feasible to achieve an interfacial layer-free high- κ film growth on Ge, an alternative physical characterization should be considered. In this work, synchrotron-radiation photoemis-

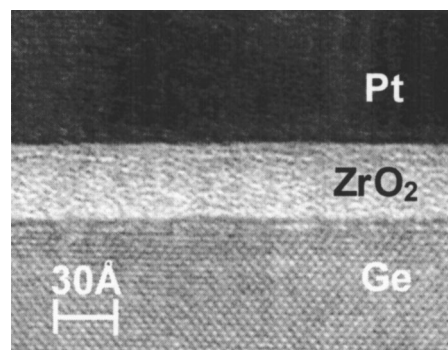


FIG. 1. Cross-sectional high-resolution transmission electron microscopy (HR-TEM) image of a sub-1.0-nm EOT Pt/ZrO₂/Ge gate stack (see Ref. 7) showing no apparent interfacial layer between the atomically abrupt high- κ dielectric and the substrate.

^{a)}Author to whom correspondence should be addressed; electronic mail: chion@stanford.edu

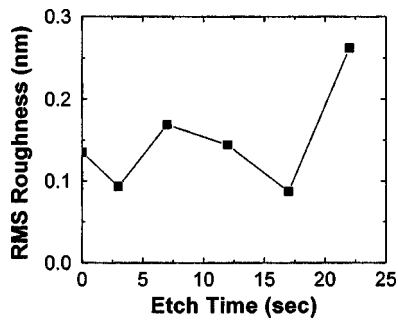


FIG. 2. ZrO_2/Ge sample surface root-mean-square roughness (R_{rms}) measured by atomic force microscopy (AFM) as a function of the etch time in 100:1 aqueous HF solution.

sion spectroscopy (SR-PES) was used due to its high surface sensitivity and fine energy resolution. Upon layer-by-layer removal of the ZrO_2 film on Ge, the compositional and chemical evolution was monitored to determine the existence of any interfacial GeO_x layer using SR-PES. In addition, the ZrO_2 -Ge interface energy-band alignment was determined by monitoring offsets in the valence-band spectra. Lastly, the impact of the interface and its band structure on the ultimate scalability of high- κ gate stacks on Ge is discussed.

II. EXPERIMENT

The ZrO_2 on Ge sample was prepared by room temperature ultraviolet-assisted ozone oxidation of sputtered thin Zr metal precursor on Ge,⁷ but without the *in situ* sputtering of Pt electrode layer to facilitate the SR-PES analysis. Prior to the ZrO_2 deposition, the Ge surface was first etched with hydrofluoric acid (HF) vapor with the intention to remove any interfacial GeO_x layer. This ZrO_2 film was expected to have an amorphous nature with a physical thickness of about 3.5 nm and an atomically abrupt interface with the Ge substrate, similar to the sample shown in Fig. 1. Next, this ZrO_2 film was etched in a layer-by-layer fashion with numerous SR-PES spectra taken between these etches. These layer-by-layer etches were carried out inside an argon (Ar)-purged glove bag attached to the analytical load-lock chamber using a 100:1 aqueous HF solution. The ZrO_2 film etch rate was about 0.2–0.3 nm/s. In order to guarantee that the wet etched ZrO_2 surfaces were smooth and pinhole-free after each HF etch, atomic force microscopy (AFM) was used⁹ to monitor the surface morphology and extract root-mean-square roughness (R_{rms}) as a function of the etch time as illustrated in Fig. 2. The R_{rms} level was maintained around 0.15 nm (<half of a monolayer) roughly before the entire ZrO_2 layer was removed, beyond which the roughness increased owing to the HF-induced Ge surface roughening. These results indicate that this wet-etching technique could provide pinhole-free surfaces throughout the layer-by-layer removal.

The synchrotron-radiation source is provided by the Stanford Positron Electron Asymmetric Ring (SPEAR) located at the Stanford Synchrotron Radiation Laboratory (SSRL). The SR-PES experiments were performed at beamline 8-1 of SSRL with a photon monochromator energy range of 20–180 eV and a photon flux spot size of $2 \times 0.5 \text{ mm}^2$ at

the sample position. During data acquisition, the analytical chamber base pressure was kept at $\sim 5 \times 10^{-11}$ Torr. The photoemission spectra were measured with a PHI model 10–360 hemispheric capacitor electron energy analyzer with the Omni Focus III small-area lens mounted on the chamber with an angle of 54° , with respect to the incoming photon beam direction. The analyzer has a multichannel detector that allows a detectable kinetic-energy (KE) range of 0–1000 eV with an energy resolution of 0.05 eV. The photoelectron take-off angle is set normal to the sample surface to maximize the depth information.

In order to maximize the SR-PES sensitivity from the sample, it is necessary to select Ge core-level peaks carefully with regards to the beamline capability. Since the available photon energy range of beamline 8-1 allows us to observe both the Ge $3d$ [with a binding energy (BE) of 29.2–29.8 eV] and Ge $3p$ (with a BE of 120.8–124.9 eV) core levels, their corresponding subshell photoelectron cross-sections should be compared. Within the photon energy range of interest, the Ge $3d$ peaks possess photoelectron cross sections at least one and a half order of magnitude larger than those of the Ge $3p$ peaks,¹⁰ and therefore the Ge $3d$ peaks were chosen to be monitored. It is worth noting that the Zr $4p$ core-level peaks also have a similar BE (27.1–28.5 eV), which may overlap with the Ge $3d$ spectra. Fortunately, the photoelectron cross sections of the Zr $4p$ signals are at least an order of magnitude lower than those of the Ge $3d$ signals, and careful peak fittings allow clear distinction between the two for our purpose.

III. RESULTS AND DISCUSSIONS

A. Interfacial layer identification and quantification

The first objective of this work was to trace the compositional and chemical evolutions within the ZrO_2 -Ge stack during the layer-by-layer wet etching of the ZrO_2 film. Due to the high surface sensitivity of the SR-PES technique, the captured core-level spectra could be utilized to discover the existence of any interfacial GeO_x layer inside the stack. The 100-eV input photon energy was selected to seize both core-level and valence-band spectra simultaneously with the same system setting. Since the etch duration (which was on the order of seconds) was difficult to control, the spectra from the two samples were interleaved together without compromising the general trend as illustrated in Fig. 3(a). Qualitatively, no Ge $3d$ core-level peak appears before the sample had been etched for ~ 11 s, which corresponds to the removal of ~ 2.8 nm of ZrO_2 . Beyond this point, the elemental Ge signals begin to appear since the inelastic mean-free paths (IMFPs)¹¹ of Ge $3d$ core-level electrons are 0.4–0.8 nm in this kinetic-energy (KE) range, which are long enough to penetrate either the ZrO_2 or the GeO_x overlayer.

From the 11-s spectrum, there exists features with binding energies (30–33 eV) higher than the Ge^{0+} peak, which could plausibly originate from either ZrO_2 or GeO_x . In an attempt to determine the source of the peak, the thicker ZrO_2 spectra (from the 3- and 6-s etched samples) were scaled and zoomed together with the 11-s spectrum, as plotted in Fig.

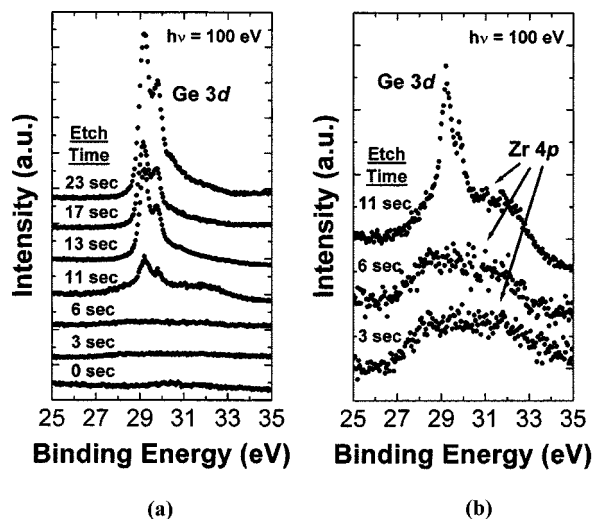


FIG. 3. (a) Evolution of the Ge 3d core-level SR-PES spectra as a function of the ZrO₂-Ge stack wet-etching time taken at a photon energy of 100 eV. (b) Scaled and zoomed spectra after 3, 6, and 11 s of etch disclosing the embedded Zr 4p core-level signals of similar binding energy.

3(b). The 0-s spectrum was not considered owing to possible surface contaminations, as previously suggested.⁹ Clearly, most of the plateau within the 11-s spectrum that has a binding energy range of 30–33 eV stems from the Zr 4p core-level signal, yet the possibility of GeO_x could not be completely neglected.

To identify any interfacial GeO_x layer and quantify its thickness if necessary, the ensemble of core-level SR-PES spectra showing the evolution of the etching sequence were first normalized to the photon beam current (I_0) to remove any real-time fluctuation in the synchrotron-radiation flux. Errors in such a computation exercise were further minimized by performing a quantification only on spectra from the same sample (not both). Given that our primary interest is the discovery of any oxidized Ge features during the evolution, the overlapping ZrO₂ signals were identified upfront and subsequently subtracted through an iterative peak-fitting procedure. In brief, the Zr 4p peaks (BE) were first located by deconvolving the spectra from the thicker ZrO₂. By incorporating these ZrO₂ signals, extensive peak fittings¹² were then carried out on the remaining spectra by assigning the Ge 3d signals with every possible oxidation states. After all the Ge 3d and Zr 4p peak (BE) positions had been defined, they were reapplied to the ensemble of evolution spectra to further refine the deconvolutions and fitted areas. Generally speaking, rigorous fitting requirements were imposed by fixing the core-level doublet peak-splitting energies and branching ratios,¹³ the Gaussian and Lorentzian linewidths, as well as the peak-energy positions,¹⁴ while freeing only the peak areas to obtain the best possible fits. As an example, Fig. 4 depicts one such fitting result of the spectra with 17-s etch with both elemental (Ge⁰⁺) and oxidized (Geⁿ⁺ where $1 \leq n \leq 4$) peaks assigned.

The areas of the fitted Ge 3d core-level peaks as a function of the etch time are summarized in Fig. 5. To illustrate the etching progress, cross-sectional schematics of the stack are also included. First of all, a sanity check on the overall

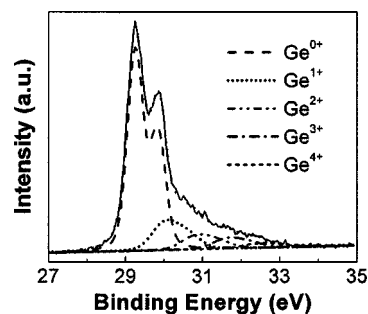


FIG. 4. Peak-fitted SR-PES spectra from the ZrO₂-Ge stack after ~17 s of etch with both elemental and oxidized Ge peaks assigned.

fitting validity was done by monitoring the substrate (Ge⁰⁺) peak evolution. The fitted peak areas increase with etch time, which is consistent with the theoretical prediction that elemental signals from a Ge substrate would be less attenuated with a thinner overlayer on top (e.g., ZrO₂ and/or GeO_x) upon etching. Next, the evolution of the oxidized Ge peaks was studied. Within the first few seconds of etching [Fig. 5(a)], all oxidized signals were absent as any possible interfacial GeO_x layer would be buried by the relatively thick ZrO₂ film above. When the ZrO₂ film got sufficiently thin [Fig. 5(b)], the more oxidized Ge signals (Geⁿ⁺ where $n \geq 2$) began to rise and reach a maximum just when the entire ZrO₂ film was removed, showing a clear evidence of an interfacial GeO_x layer within the ZrO₂-Ge stack. Further etches would start to consume the GeO_x layer [Fig. 5(c)] and cause the more oxidized Ge signal intensity to fall back down. Once all GeO_x were removed [Fig. 5(d)], the oxidized Ge signals increased slightly again with the least oxidized peak (Ge¹⁺) dominating. This reappearance of the oxidized Ge signature may be due to the Ge surface reoxidation right after a complete GeO_x removal even inside the Ar-purged glove bag and formation of substoichiometric surface oxides. Finally, the questionable continued increase of the Ge⁰⁺ intensity even after the complete GeO_x removal [Fig. 5(d)] could be attributed to the surface roughening of the Ge surface, as observed in Fig. 2.

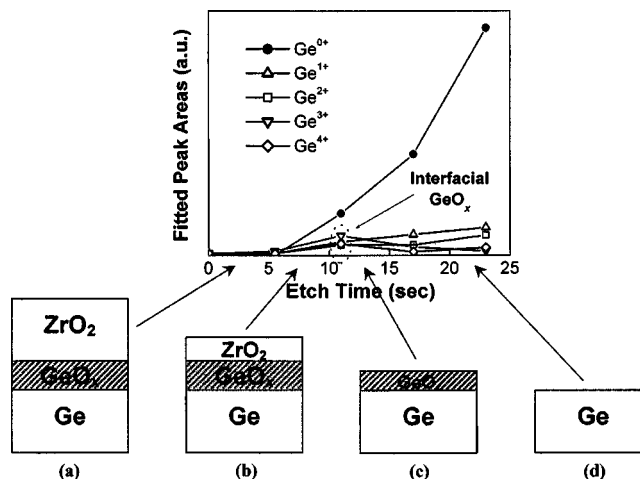


FIG. 5. Extracted core-level Ge 3d fitted peak areas as a function of etch time. Cross-sectional schematics of the stack are also included to illustrate the layer-by-layer etching progress.

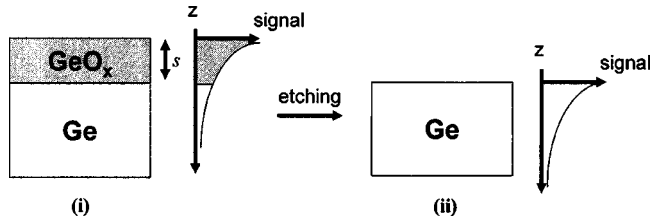


FIG. 6. Illustrations of escape depth calculation of the photoelectrons from Ge substrate at two different time points: (i) right around the complete ZrO_2 removal and (ii) right around the complete GeO_x removal.

Next, the extraction of the interfacial GeO_x layer thickness was done by first computing the escape depth of photoelectrons from the Ge substrate, as illustrated in Fig. 6. In doing so, the extraction time points throughout the evolution were judiciously selected to simplify the calculation process: (i) right around the complete ZrO_2 removal and (ii) right around the complete GeO_x removal. Thus, the fitted peak area right after the ZrO_2 removal, $N_{\text{Ge(i)}}$, could be expressed in

$$N_{\text{Ge(i)}} \propto e^{-s/\lambda_{\text{GeO}_x}} \int_s^\infty e^{-z/\lambda_{\text{Ge}}} dz = \lambda_{\text{Ge}} e^{-s/\lambda_{\text{GeO}_x}} e^{-s/\lambda_{\text{Ge}}}, \quad (1)$$

and the fitted peak area right after the GeO_x removal, $N_{\text{Ge(ii)}}$, could be related using

$$N_{\text{Ge(ii)}} \propto \int_0^\infty e^{-z/\lambda_{\text{Ge}}} dz = \lambda_{\text{Ge}}, \quad (2)$$

where s is the GeO_x thickness, and λ_{GeO_x} and λ_{Ge} are the electron IMFPs in GeO_x and Ge, respectively. By substituting Eq. (2) into Eq. (1), the GeO_x thickness could thus be extracted using

$$s = \frac{\lambda_{\text{Ge}} \lambda_{\text{GeO}_x}}{\lambda_{\text{Ge}} + \lambda_{\text{GeO}_x}} \ln \left(\frac{N_{\text{Ge(ii)}}}{N_{\text{Ge(i)}}} \right). \quad (3)$$

The λ_{Ge} is estimated to be about 0.44 nm and λ_{GeO_x} could range between 0.4–0.8 nm at our KE range.¹¹ Taking into account any potential errors in the determination of extraction time point and uncertainty in λ_{GeO_x} , the interfacial GeO_x thickness is calculated to be 0.19–0.36 nm. Since this is less than a complete monolayer thickness of GeO_x , the oxidized Ge signature was therefore attributed to a possible Zr–O–Ge interfacial bonding configuration. Moreover, the interfacial GeO_x thicknesses, as determined by SR-PES, are comparable to those obtained by an angle-resolved x-ray photoemission study on similar gate stacks.¹⁵

B. Interface energy-band alignment

In addition to the possession of an *ultrathin* interfacial layer, having sufficiently large barrier heights for electron and hole injection would be considered as an equally important high- κ dielectric qualification criterion to lower gate leakage for better scalability. Among other techniques, photoemission is one of the most reliable methods to study these systems. In particular, offsets in the valence-band spectra could be monitored to map out the interface energy-band alignment for many high- κ on Si and Ge stacks,^{16–18} and its

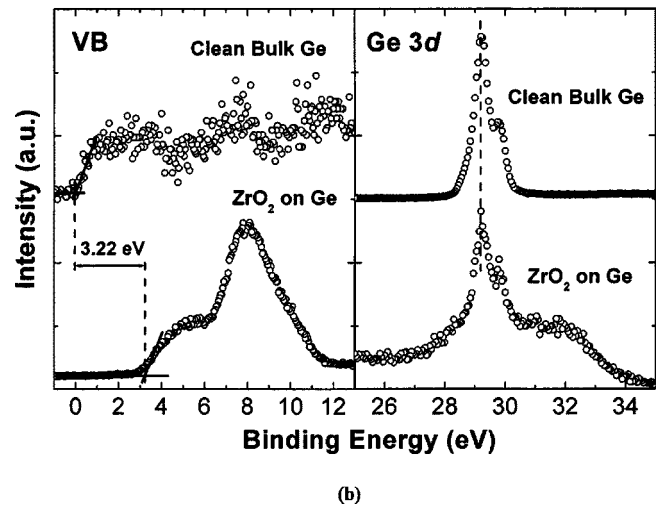
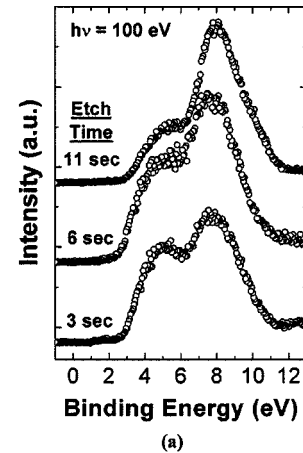


FIG. 7. (a) Valence-band photoemission spectra from thicker ZrO_2 captured during the etching evolution. (b) Valence-band spectra (left) from a clean bulk Ge sample and the ZrO_2 -Ge stack after 11 s of etch with their corresponding Ge 3d core-level peaks aligned (right).

application to our ZrO_2 -Ge interface is the focus of this section.

The basic principle is to first locate the valence-band edge (BE position) from those thicker ZrO_2 photoemission spectra throughout the evolution, as shown in Fig. 7(a), and then compare with the valence-band edge from a clean bulk Ge. For an accurate valence-band-offset measurement, any energy shift induced by a sample surface charging during photoemission should be corrected by aligning to the Ge 3d core-level peaks. Since a definitive Ge^{0+} signal had only been discerned from the 11-s spectrum in Fig. 3(b), this spectrum was chosen for the ZrO_2 valence-band-offset estimation as detailed in Fig. 7(b). The clean bulk Ge spectra were prepared by *in situ* heating of a bare Ge substrate to 700 °C for ~25 min to desorb any surface native oxides¹⁹ after pumping down the inside of the analytical chamber. The valence-band edge was determined to be the point of intersection of a “best” straight line fit to represent the decay in the valence-band spectrum and the baseline.^{16–18} After aligning their corresponding Ge^{0+} core-level peaks, the valence-band offset (ΔE_V) between bulk Ge and ZrO_2 was found to be 3.22 eV, as highlighted in Fig. 7(b), a value that is comparable to the 3.36 eV obtained by x-ray photoemission spectroscopy.¹⁸

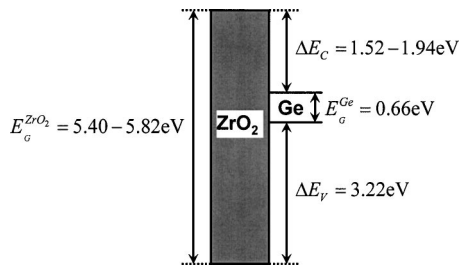


FIG. 8. Energy-band diagram of the ZrO_2 -Ge structure inferred from the SR-PES measurements.

Before the entire ZrO_2 -Ge interface energy-band alignment could be determined, the energy-band gap of ZrO_2 needed to be researched in literature. From those reports on both amorphous and polycrystalline ZrO_2 that were deposited using various methods on either Si or Ge, the energy-band gap of ZrO_2 ($E_G^{\text{ZrO}_2}$) was experimentally measured to be 5.40–5.82 eV.^{16,18,20} Together with the interface data from the last section, the energy-band diagram of the ZrO_2 -Ge structure was constructed as displayed in Fig. 8. Taking the Ge energy-band gap (E_G^{Ge}) to be 0.66 eV at 300 K,²¹ the conduction-band offset (ΔE_C) is deduced to be 1.52–1.94 eV.

In order to calculate the theoretical conduction-band offset amount, one has to first realize that the band alignment between two semiconductors is controlled by the charge transfer across the interface,²² similar to the Schottky barrier formation. The resulting interface dipoles, associated with quantum-mechanical tunneling, modify the band alignment as governed by the electron affinity rule. Applying to our ZrO_2 -Ge heterostructure, the ΔE_C could be predicted²³ using the following expression:

$$\Delta E_C = \chi_{\text{Ge}} - \chi_{\text{ZrO}_2} + (S - 1)(\Phi_{\text{CNL,Ge}} - \Phi_{\text{CNL,ZrO}_2}), \quad (4)$$

where χ_{Ge} and χ_{ZrO_2} are the electron affinities of Ge and ZrO_2 , respectively, $\Phi_{\text{CNL,Ge}}$ and $\Phi_{\text{CNL,ZrO}_2}$ are the charge neutrality levels of Ge and ZrO_2 , respectively, and S is an empirically fitted slope accounting for dielectric screening. Employing the values reported in Refs. 21 and 22, the theoretical ΔE_C was calculated to be 1.63 eV, which is in good agreement with our SR-PES measurements.

C. Scalability of high- κ on Ge stacks

In the previous sections, a submonolayer GeO_x interface and a conduction-band offset in excess of 1.5 eV have been identified on the ZrO_2 -Ge system of interest. Both of these characteristics are, in effect, hinting that a better scalability could be achieved with the high- κ gate stacks on Ge than on Si.

On one hand, the usual interfacial SiO_x layer thickness in high- κ gate stacks on Si is on the order of 0.5–1.0 nm,⁸ which also sets the EOT scaling limit. However, this low-permittivity interfacial layer could largely be removed or eliminated when these high- κ gate stacks are integrated onto Ge, presenting an alternate direction to further extend the EOT scaling potential. In addition to the *ultrathin* interfacial layer demonstrated in the present study, hafnia (HfO_2)

formed on Ge either by reactive sputtering²⁴ or metal-organic chemical vapor deposition²⁵ also exhibited much thinner interfacial layers than did the hafnia on Si. Theoretically, the formation of such interfacial layers is unlikely when high- κ dielectrics are put in contact with Ge, given the large Gibbs free-energy change for such a process,²⁶ despite the fact that the oxygen vacancies in these high- κ materials would tend to inject oxygen atoms^{27,28} to the high- κ dielectric/Ge interface.

On the other hand, a lower conduction-band offset would result when the same high- κ dielectric is deposited on Si than on Ge. This hypothesis is based on a simple calculation using Eq. (4), given the larger value of Si charge neutrality level ($\Phi_{\text{CNL,Si}}$)²² and similar Si electron affinity (χ_{Si}),²¹ as compared to Ge. In fact, this argument is further reinforced by the reported conduction-band offsets of less than 1.5 eV for common high- κ dielectrics on Si from both experimental measurements^{16,17,29} and theoretical predictions.²³ Therefore, the larger conduction-band offset from our ZrO_2 -Ge stack has a distinct advantage of suppressing gate-leakage current due to an inverse exponential dependency of electron barrier height on the electron direct tunneling transport.²¹

IV. CONCLUSIONS

Given the limitation of the conventional TEM, we have introduced the use of SR-PES to determine the compositional and chemical evolutions within the ZrO_2 -Ge stack during layer-by-layer wet etching of the ZrO_2 film. In doing so, the existence of oxidized Ge features at the interface have been identified. After extensive peak fittings of the core-level spectra, the interfacial GeO_x thickness has been calculated to be 0.19–0.36 nm. This submonolayer signature could possibly arise from a Zr-O-Ge interfacial bonding configuration rather than from a distinct and continuous interfacial layer.

Additionally, the energy-band diagram of the ZrO_2 -Ge structure was constructed by monitoring offsets in the SR-PES valence-band spectra. With errors in the ZrO_2 energy band gap determination, the conduction-band offset has been deduced to be 1.52–1.94 eV. Combining all the above observations, the high- κ gate stack integration on Ge shows a better EOT scalability than does the same integration on Si due to the much thinner interfacial layer and larger electron tunneling barrier.

ACKNOWLEDGMENTS

The authors are grateful to Dr. Shriram Ramanathan and Professor Paul C. McIntyre for fruitful discussions and assistance with zirconia deposition. C.O.C. would also like to acknowledge the support of the Intel Foundation Ph.D. fellowship. Finally, this work was performed at the Stanford Synchrotron Radiation Laboratory, a national user facility operated by Stanford University on behalf of the U.S. Department of Energy, Office of Basic Energy Sciences.

¹The International Technology Roadmap for Semiconductors, Semiconductor Industry Association, 2003.

²M. L. Lee *et al.*, Appl. Phys. Lett. **79**, 3344 (2001).

³C. O. Chui, H. Kim, D. Chi, B. B. Triplett, P. C. McIntyre, and K. C. Saraswat, *Technical Digest International Electron Devices Meeting (IEEE)*, San Francisco, CA, 2002, p. 437.

- ⁴H. Shang *et al.*, *Technical Digest International Electron Devices Meeting* (IEEE, San Francisco, CA, 2002), p. 441.
- ⁵M. Lundstrom, *IEEE Electron Device Lett.* **18**, 361 (1997).
- ⁶J. Bardeen and W. H. Brattain, *Phys. Rev.* **74**, 230 (1948).
- ⁷C. O. Chui, S. Ramanathan, B. B. Triplett, P. C. McIntyre, and K. C. Saraswat, *IEEE Electron Device Lett.* **23**, 473 (2002).
- ⁸G. D. Wilk, R. M. Wallace, and J. M. Anthony, *J. Appl. Phys.* **89**, 5243 (2001).
- ⁹C. O. Chui, D.-I. Lee, A. A. Singh, D. Chi, P. C. McIntyre, P. A. Pianetta, and K. C. Saraswat, *Abstract Spring Meeting* (MRS, San Francisco, CA, 2004), p. 49.
- ¹⁰J. J. Yeh and I. Lindau, *At. Data Nucl. Data Tables* **32**, 1 (1985).
- ¹¹*NIST Electron Inelastic-Mean-Free-Path Database 71 (Ver. 1.1)*, National Institute of Standards and Technology, 2000.
- ¹²A. Herrera-Gómez, F. S. Aguirre-Tostado, Y. Sun, P. Pianetta, Z. Yu, D. Marshall, R. Droopad, and W. E. Spicer, *J. Appl. Phys.* **90**, 6070 (2001).
- ¹³X. Yang, R. Cao, J. Terry, and P. Pianetta, *J. Vac. Sci. Technol. B* **10**, 2013 (1992).
- ¹⁴D. Schmeisser, R. D. Schnell, A. Bogen, F. J. Himpsel, D. Rieger, G. Landgren, and J. F. Morar, *Surf. Sci.* **172**, 455 (1986).
- ¹⁵D. Chi, C. O. Chui, K. C. Saraswat, B. B. Triplett, and P. C. McIntyre, *J. Appl. Phys.* **96**, 813 (2004).
- ¹⁶S. Miyazaki, *J. Vac. Sci. Technol. B* **19**, 2212 (2001).
- ¹⁷S. Sayan, E. Garfunkel, and S. Suzer, *Appl. Phys. Lett.* **80**, 2135 (2002).
- ¹⁸S. J. Wang *et al.*, *Appl. Phys. Lett.* **85**, 4418 (2004).
- ¹⁹K. Prabhakaran, F. Maeda, Y. Watanabe, and T. Ogino, *Appl. Phys. Lett.* **76**, 2244 (2000).
- ²⁰M. Houssa, M. Tuominen, M. Naili, V. Afanas'ev, A. Stesmans, S. Haukka, and M. M. Heyns, *J. Appl. Phys.* **87**, 8615 (2000).
- ²¹S. M. Sze, *Physics of Semiconductor Devices*, 2nd ed. (Wiley, New York, 1981).
- ²²J. Tersoff, *Phys. Rev. B* **30**, 4874 (1984).
- ²³J. Robertson, *J. Vac. Sci. Technol. B* **18**, 1785 (2000).
- ²⁴K. Kita, K. Kyuno, and A. Toriumi, *Appl. Phys. Lett.* **85**, 52 (2004).
- ²⁵S. Van Elshocht *et al.*, *Appl. Phys. Lett.* **85**, 3824 (2004).
- ²⁶H. Kim, C. O. Chui, K. C. Saraswat, and P. C. McIntyre, *Appl. Phys. Lett.* **83**, 2647 (2003).
- ²⁷K. Shiraishi *et al.*, *Technical Digest Symposium on VLSI Technology* (IEEE, Piscataway, NJ, 2004), p. 108.
- ²⁸H. Takeuchi, H. Y. Wong, D. Ha, and T.-J. King, *Technical Digest International Electron Devices Meeting* (IEEE, San Francisco, CA, 2004), p. 829.
- ²⁹M. Oshima *et al.*, *Appl. Phys. Lett.* **83**, 2172 (2003).